Extended Spherical Harmonic Expansion Using Multipolar Bases Of Equivalent Magnetic Sources On Arbitrary Surfaces

Gauthier Derenty-Camenen, Alexis Lepot, Olivier Chadebec, Olivier Pinaud, L-L. Rouve, Steeve Zozor

Extended Spherical Harmonic Expansion Using Multipolar Bases Of Equivalent Magnetic Sources On Arbitrary Surfaces

Gauthier Derenty-Camenen[1,2], Alexis Lepot[3], Olivier Chadebec[1], Olivier Pinaud[1], Laure-Line Rouve[1] and Steeve Zozor[2]
[1]Univ. Grenoble Alpes, CNRS, Grenoble INP, G2Elab, 38000 Grenoble, France
[2]Univ. Grenoble Alpes, CNRS, Grenoble INP, GIPSA-Lab, 38000 Grenoble, France
[3]DGA Techniques navales Brest, CC42, 29240 Brest, France

Abstract

Purpose - The purpose of this paper is to propose a compact model to represent the magnetic field outside the sources. This model provides the multipolar ordering of a spherical harmonic expansion far from the source, while being valid in its close proximity.

Design/methodology/approach - We investigate equivalent surface sources that enable to compute the field very close to any chosen surface that encloses the source. Then we present a method to find an appropriate initial basis and its associated inner product that allow to construct multipolar harmonic bases for these equivalent sources, where any vector of order k produces a field that decreases at least as fast as the field produced by a multipole of order k. Finally those bases are numerically implemented to demonstrate their performances, both far from the source and in its close proximity.

Findings - The charge distribution and normal dipole distribution are well-suited to construct multipolar harmonic bases of equivalent sources. These bases can be described by as few parameters as the decreasing spherical harmonic expansion. Comparison with other numerical models shows its ability to compute the field both far from the source and close to it.

Originality - A basis for normal dipole distribution has already been described in the literature. This paper presents a general method to construct a multipolar basis for equivalent sources and uses it to construct a basis for single-layer potential.

Keywords - Double-layer potential, multipolar expansion, near magnetic field computation, single-layer potential

1 Introduction

For various applications (electromagnetic compatibility (Van Hoang et al. 2014), human exposure (Tavernier et al. 2021), ship silencing (Chavin-Collin et al. 2021)), the magnetic field produced by a device must be determined all around it. Depending on its constitutive complexity, some lacking information about the sources may not allow a direct numerical modelling with usual numerical methods, and other alternatives must be found. Identification of a compact model (i.e. using a limited number of representative coefficients) from close magnetic measurements is a common inverse problem approach (Whaler and Gubbins 1981).

Classically, the external field may be represented by a multipolar expansion using the decreasing spherical harmonic functions (DSHF). The sources are then equivalent to a set of multipoles (e.g., dipole, quadrupole), each multipole being associated to a spatial harmonic which presents a specific spatial decreasing law (e.g., $1/r^3$, $1/r^4$), allowing a natural truncation of the expansion at a given distance and leading to an accurate model with only a few degrees of freedom (DoF). Nevertheless, DSHF representation is only valid outside the Brillouin sphere (BS) (Costin et al. 2022), the smallest sphere that encloses all the sources (see Fig. 1), and cannot be used in the close vicinity of the device.

On the other hand, equivalent magnetic sources, such as charge distribution (CD) and/or normal dipole distribution (NDD), located on any arbitrary surface that encloses all the sources, are very general and do not have this limitation. However they are not specifically linked to a spatial decreasing law and may need a high number of DoF to represent the field accurately.

In this paper, we propose to mix the two previous models in order to provide new multipolar bases for surface equivalent source representations. This proposition has already been made for NDD in previous work (Legris 1996). It is now revisited to present its extension to CD, while highlighting the generalization of the bases construction method. Thanks to this mixed model, the main interesting advantages of initial ones are preserved. On one hand, the surfacic description enables to localize sensors close to the sources. On the other hand, the construction of the multipolar basis ensures that each harmonic of the equivalent sources produces a field that decreases at least like the mulipole of the same order, outside the Brillouin sphere. Even if this mixed model is clearly motivated by the problem of source identification in an inverse problem context, the aim of this paper specifically addresses the question of its performances for a direct problem approach.

Firstly, the properties of the Spherical Harmonic Model, based on the DSHF, are reminded in Section 2 as well as the ones of equivalent surface distributions (boundary conditions, CD and NDD) in Section 3. Then the construction and the implementation of the multipolar bases for CD and NDD are detailed in Section 4. Finally in Section 5, the proposed model is tested through an analytical example and its performances compared to the ones of more classical models inside the BS (NDD and CD distributions, boundary conditions approach) and outside (Spherical Harmonic Model).

2 Decreasing Spherical Harmonic Functions

Outside any surface enclosing magnetic sources, if the exterior volume is simply connected, the magnetic field derives from a scalar potential ϕ that satisfies the Laplace equation. In spherical coordinates, outside the BS, we can express this potential (and the associated field $\boldsymbol{H}$) at any point of spherical coordinates (r, θ, φ) in their multipolar expansion using the Decreasing Spherical Harmonic Functions (DSHF) (Stratton 1941, pp. 179–183):

$$\phi(r,\theta,\varphi) = \frac{1}{4\pi} \sum_{k=1}^{\infty} \sum_{m=-k}^{k} a_{km} \frac{Y_k^m(\theta,\varphi)}{r^{k+1}} \tag{1}$$

$$\boldsymbol{H}(r,\theta,\varphi) = \frac{-1}{4\pi} \sum_{k=1}^{\infty} \sum_{m=-k}^{k} a_{km} \boldsymbol{\nabla} \left(\frac{Y_k^m(\theta,\varphi)}{r^{k+1}} \right) \tag{2}$$

where a_{km} are the spherical harmonic coefficients. Y_k^m is the spherical harmonic function of order k and degree m constructed with the associated Legendre polynomial $P_k^{|m|}$ of order $|m|$ and degree k:

$$Y_k^m(\theta,\varphi) = \sqrt{\frac{(k-|m|)!}{(k+|m|)!}} P_k^{|m|}(\cos(\theta)) \begin{cases} \sqrt{2}\cos(m\varphi) & \text{if } m > 0 \\ 1 & \text{if } m = 0 \\ \sqrt{2}\sin(|m|\varphi) & \text{if } m < 0 \end{cases} \tag{3}$$

For a chosen center of expansion, the spherical harmonic coefficients a_{km} depend only on the source, $Y_k^m(\theta,\varphi)/r^{k+1}$ being the DSHF with the typical spatial decreasing law $1/r^{k+1}$ associated to the multipole of order k. Thanks to this specific decreasing law any desired level of precision can be achieved at a given distance by truncation of the DSHF basis. A well-known and useful property of this representation is the fact that a magnetic source is equivalent to a dipole at a long distance. More generally, by truncating Eq. (2) at a maximum order K, this mathematical expansion approximates the field produced by multipoles, outside the Brillouin sphere, in a very compact and ordered way, as it requires the determination of only $K(K+2)$ coefficients a_{km}.

3 Equivalent sources on arbitrary surfaces

3.1 Boundary conditions

Let S be any arbitrary surface enclosing all the sources as in Figure 1. For any source, by knowing the scalar magnetic potential on this surface ϕ_S and the normal field $H_n = \boldsymbol{H} \cdot \boldsymbol{n}$ we can compute

the scalar magnetic potential ϕ (and the associated field $\boldsymbol{H}$) everywhere outside the chosen surface (Stratton 1941, pp. 165–167).

The scalar potential is expressed by using Green's function G or its normal derivative $\partial_n G$. The Green's function for any two points M and P in 3D is given by:

$$G(P, M) = \frac{1}{4\pi} \frac{1}{\|\boldsymbol{PM}\|} \tag{4}$$

its normal derivative, with $\boldsymbol{n}$ the outward-pointing normal vector, is:

$$\partial_n G(P, M) = -\boldsymbol{n}(M) \cdot \boldsymbol{\nabla}_M G(P, M) = \frac{1}{4\pi} \frac{\boldsymbol{n}(M) \cdot \boldsymbol{PM}}{\|\boldsymbol{PM}\|^3} \tag{5}$$

with $\boldsymbol{\nabla}_M$ the gradient with respect to the coordinates of the point M.

The scalar magnetic potential at any point P exterior to S is then expressed using the third Green's identity:

$$\phi(P) = -\int_{M \in S} \left(H_n(M)\, G(P, M) + \phi_S(M)\, \partial_n G(P, M) \right) \mathrm{d}S \tag{6}$$

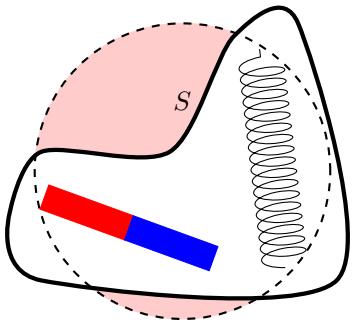

Figure 1: 2D illustration of the choice of an arbitrary surface S enclosing all the sources, currents and magnetization. In red the domain outside the surface which is inside the Brillouin sphere.

Source: Figure created by authors

The integral giving the potential from the normal field H_n is called the single-layer potentials and the integral giving the the potential from the the surface potential ϕ_S is called the double-layer potentials. Their names comes from the fact that these operators are the ones used to compute the potential from a single-layer or a double-layer of charges, being equivalent respectively to a CD and a NDD.

Let us notice that the surface normal field and the surface potential are linked by the third Green identity when the point P belongs to the surface, and that the knowledge of only one of the two quantities enables to determine the field outside the sources. When the surface is discretized by a mesh, this means that the normal field, the potential or a relation between the two must be known on each mesh element.

3.2 Equivalent charge and normal dipole distributions

Instead of using the boundary conditions, we can define on the surface S a charge distribution σ or a normal dipole distribution τ that produce the same magnetic field outside the surface (Stratton 1941, pp. 187–192).

For these two distributions, the magnetic scalar potential can be computed using one the single-layer or double-layer potentials as in (6). At any point P exterior to S, the magnetic scalar potential can be expressed as:

$$\phi(P) = \int_{M \in S} \sigma(M)\, G(P, M)\, \mathrm{d}S \tag{7}$$

$$\phi(P) = \int_{M \in S} \tau(M)\, \partial_n G(P, M)\, \mathrm{d}S \tag{8}$$

When crossing the surface, the magnetic scalar potential is continuous for the CD but not for the NDD. We can link the boundary condition on the potential ϕ_S to those distributions, at any point P_S on the surface S:

$$\phi_S(P_S) = \int_{M \in S} \sigma(M)\, G(P_S, M)\, \mathrm{d}S \tag{9}$$

$$= \frac{1}{2}\tau(P_S) + \int_{M \in S} \tau(M)\, \partial_n G(P_S, M)\, \mathrm{d}S \tag{10}$$

For any given enclosed source, we can find a charge distribution σ and a normal dipole distribution τ that produces the same field. Those two distributions can be seen as the boundary conditions of a function u which is harmonic inside the surface S (i.e. $\Delta u = 0$) (Bonnet 1995; Kybic et al. 2005). The NDD is the boundary value of this function u and the CD is its normal derivative:

$$\forall M \in S \begin{cases} \tau(M) = u(M) & (11) \\ \sigma(M) = \partial_n u(M) & (12) \end{cases}$$

This relation means that the third Green's identity can be applied on the surface S for these two distributions for any point P_S on the surface:

$$\frac{1}{2}\tau(P_S) = \int_{M\in S} \big(\sigma(M)\, G(P_S, M) - \tau(M)\, \partial_n G(P_S, M)\big)\, \mathrm{d}S \tag{13}$$

$$\frac{1}{2}\tau(P_S) + \int_{M\in S} \tau(M)\, \partial_n G(P_S, M)\mathrm{d}S = \int_{M\in S} \sigma(M)\, G(P_S, M)\, \mathrm{d}S \tag{14}$$

We can note that this equation can also be found directly from (9) and (10).

4 Multipolar bases of equivalent sources on arbitrary surfaces

In this section, the multipolar bases are described for both NDD and CD. Firstly, for the sake of clarity, we directly provide our main result, which is how these bases are constructed. Then, we explain our motivations for the choice of the specific initial bases and of the inner product used both to othonormalize them and to obtain specific decreasing behavior according to each harmonics. More specifically, we will exhibit how the new source multipolar coefficients are linked to the spherical harmonic coefficients a_{km}. Regarding the numerical implementation, we will mainly pay attention to the quality of the orthonormalization procedure and its impact on the model accuracy.

4.1 Construction of the multipolar bases

Having the DSHF model in mind, our goal is to construct two surface harmonic bases $\{\sigma_{km}\}$ and $\{\tau_{km}\}$ to represent respectively CD and NDD:

$$\sigma(M) = \sum_{k=1}^{\infty} \sum_{m=-k}^{k} c_{km}\, \sigma_{km}(M) \tag{15}$$

$$\tau(M) = \sum_{k=1}^{\infty} \sum_{m=-k}^{k} c_{km}\, \tau_{km}(M) \tag{16}$$

with c_{km} the source harmonic coefficients, σ_{km} and τ_{km} the vectors of the bases, of order k and degree m, and M any point of the chosen arbitrary surface S. Let us notice that for a same source the coefficients c_{km} are the same for both representations, we will show this in paragraph 4.5.1.

Those bases $\{\sigma_{km}\}$ and $\{\tau_{km}\}$ (see Fig. 2) are constructed by orthonormalizing initial bases $\{\sigma^0_{km}\}$ and $\{\tau^0_{km}\}$ with respect to specific inner products $\langle\sigma_1|\sigma_2\rangle$ and $\langle\tau_1|\tau_2\rangle$. The source harmonic coefficients c_{km} are then defined for a known CD σ or NDD τ as:

$$c_{km} = \langle\sigma|\sigma_{km}\rangle = \langle\tau|\tau_{km}\rangle \tag{17}$$

The initial bases are defined using the increasing spherical harmonic functions on the surface, at every point (r, θ, φ) of the surface S:

$$\sigma^0_{km}(r,\theta,\varphi) = \partial_n \left(r^k Y^m_k(\theta,\varphi)\right) \qquad \forall (r,\theta,\varphi) \in S \tag{18}$$

$$\tau^0_{km}(r,\theta,\varphi) = r^k Y^m_k(\theta,\varphi) \qquad \forall (r,\theta,\varphi) \in S \tag{19}$$

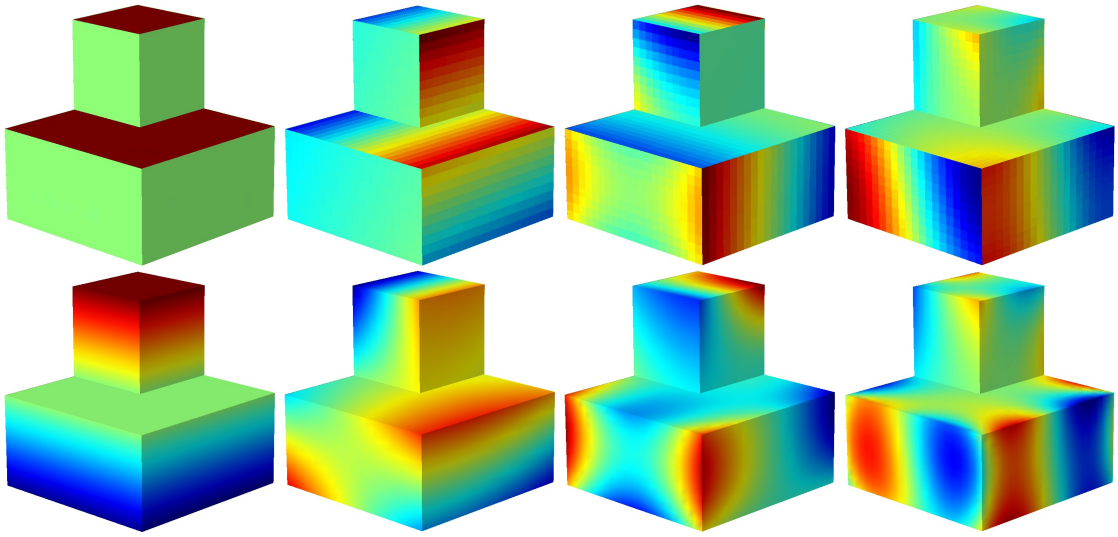

Figure 2: Illustration of vectors from the two bases $\{\sigma_{km}\}$ (above) and $\{\tau_{km}\}$ (below). With from left to right: $k = 1$ and $m = 1$, $k = 2$ and $m = -2$, $k = 3$ and $m = 2$, $k = 4$ and $m = -1$.

Source: Figure created by authors

The inner products are defined as:

$$\langle \sigma_1 | \sigma_2 \rangle = V \int_{M \in S} \tau[\sigma_1](M)\sigma_2(M)\, \mathrm{d}S \tag{20}$$

$$\langle \tau_1 | \tau_2 \rangle = V \int_{M \in S} \sigma[\tau_1](M)\tau_2(M)\, \mathrm{d}S \tag{21}$$

where $\sigma[\tau_1]$ is the CD on the surface S that produces the same field as τ_1 outside of S and $\tau[\sigma_1]$ is the NDD on the surface S that produces the same field as σ_1 outside of S and that satisfy $\int_{M\in S} \tau[\sigma_1](M)\, \mathrm{d}S = 0$ (the NDD is defined up to a uniform distribution). V is the volume contained in the surface S.

This construction ensures that any vector of order k taken from the bases$\{\sigma_{km}\}$ and $\{\tau_{km}\}$ produces a scalar potential that decreases at least as fast as $1/r^{k+1}$. In the following, we will show why we chose these initial bases and their associated inner product in order to construct the proposed multipolar bases that meets the desired property.

4.2 Definition of the objective

Our objective is to build these bases such that basis vector of order k, σ_{km} or τ_{km}, produces a potential outside the BS with a decreasing law at least of $1/r^{k+1}$. This property means that:

$$a_{k'm'}[\sigma_{km}] = a_{k'm'}[\tau_{km}] = 0 \quad \text{if } k' < k. \tag{22}$$

where $a_{k'm'}[\sigma_{km}]$ (respectively $a_{k'm'}[\tau_{km}]$) is the spherical harmonic coefficient of order k' and degree m' obtained from the spherical multipolar decomposition (1) of the scalar potential ϕ_{km} produced by the vector σ_{km} (7) (respectively τ_{km}). If condition (22) is respected, then the potential ϕ_{km} at any point (r, θ, φ) outside the BS can be written:

$$\phi_{km}(r, \theta, \varphi) = \frac{1}{4\pi} \sum_{k'=k}^{\infty} \sum_{m'=-k'}^{k'} a_{k'm'}[\sigma_{km}] \, \frac{Y_{k'}^{m'}(\theta, \varphi)}{r^{k'+1}} \tag{23}$$

To achieve this condition, we will construct the desired bases $\{\sigma_{km}\}$ and $\{\tau_{km}\}$ by orthonormalizing initial bases $\{\sigma_{km}^0\}$ and $\{\tau_{km}^0\}$ with appropriate inner products and a triangularisation orthonormalization method (such as Gram-Schmidt, Householder or Givens). The bases and inner products are

chosen so that we can write:

$$a_{k'm'}[\sigma_{km}] \propto \left\langle \sigma^0_{k'm'} | \sigma_{km} \right\rangle \tag{24}$$

$$a_{k'm'}[\tau_{km}] \propto \left\langle \tau^0_{k'm'} | \tau_{km} \right\rangle \tag{25}$$

with $\langle . | . \rangle$ the appropriate inner products.

The verification of condition (22) is then a direct consequence of (24) and (25) because of the orthogonality property between the basis $\{\sigma^0_{km}\}$ and the orthonormal basis $\{\sigma_{km}\}$. Indeed a vector from $\{\sigma_{km}\}$ is orthogonal to all the previous vectors of $\{\sigma^0_{km}\}$. This property is a consequence of the orthonormalization process and is independent from the choice of inner product. In particular we have:

$$\left\langle \sigma^0_{k'm'} | \sigma_{km} \right\rangle = 0 \text{ if } k' < k \tag{26}$$

The same property applies also for $\{\tau^0_{km}\}$ and $\{\tau_{km}\}$ as it is a general consequence of the orthonormalization process.

4.3 Spherical harmonic coefficients due to equivalent sources

In order to find an initial basis and an inner product for each representation, we express the spherical harmonic coefficients a_{km} for each equivalent source. These expressions will guide the choices of initial bases and inner products.

The spherical harmonic coefficients associated to CD and NDD are found using Green's function in spherical coordinates (Cohl et al. 2001). For two points in spherical coordinates $P(r_P, \theta_P, \varphi_P)$ and $M(r_M, \theta_M, \varphi_M)$, if $r_P > r_M$, we can rewrite (4) as:

$$G(P, M) = \frac{1}{4\pi} \sum_{k=0}^{\infty} \sum_{m=-k}^{k} \frac{r_M^k}{r_P^{k+1}} Y_k^m(\theta_M, \varphi_M) Y_k^m(\theta_P, \varphi_P) \tag{27}$$

Inserting (27) into (7) and (8) for a point P outside the BS, we identify the spherical harmonic coefficients as defined in (1):

$$a_{km}[\sigma] = \int_{M \in S} r_M^k Y_k^m(\theta_M, \varphi_M)\, \sigma(M)\, \mathrm{d}S \tag{28}$$

$$a_{km}[\tau] = \int_{M \in S} \partial_n \left(r_M^k Y_k^m(\theta_M, \varphi_M) \right)\, \tau(M)\, \mathrm{d}S \tag{29}$$

4.4 Choice of initial basis and inner product

Given the expressions (28) and (29) and the fact that CD and NDD can been seen as the boundary conditions of a function which is harmonic inside the surface, we would like to use the increasing spherical harmonic function basis to construct the initial bases for CD and NDD (we can notice with (11) and (12) that the vectors from the two bases of same order and degree produces the same field):

$$\sigma^0_{km}(r, \theta, \varphi) = \partial_n \left(r^k Y_k^m(\theta, \varphi) \right) \qquad \forall (r, \theta, \varphi) \in S \tag{30}$$

$$\tau^0_{km}(r, \theta, \varphi) = r^k Y_k^m(\theta, \varphi) \qquad \forall (r, \theta, \varphi) \in S \tag{31}$$

From the choice of the bases, we can now write (28) and (29) as:

$$a_{k'm'}[\sigma_{km}] = \int_{M \in S} \tau^0_{k'm'}(M) \sigma_{km}(M)\, \mathrm{d}S \tag{32}$$

$$a_{k'm'}[\tau_{km}] = \int_{M \in S} \sigma^0_{k'm'}(M) \tau_{km}(M)\, \mathrm{d}S \tag{33}$$

With these initial bases, (24) and (25) are satisfied using the inner products defined in (Legris 1996):

$$\langle \sigma_1 | \sigma_2 \rangle = \alpha \int_{M \in S} \tau[\sigma_1](M) \sigma_2(M) \, \mathrm{d}S \tag{34}$$

$$\langle \tau_1 | \tau_2 \rangle = \alpha \int_{M \in S} \sigma[\tau_1](M) \tau_2(M) \, \mathrm{d}S \tag{35}$$

where α can be any well-chosen strictly positive coefficient.

Notice that for two pairs of CD and NDD (σ_1, τ_1) and (σ_2, τ_2) such that in each pair the fields produced by σ and τ are the same, using the symmetry of the inner product it appears that the inner products (34) and (35) are equal:

$$\langle \sigma_1 | \sigma_2 \rangle = \langle \tau_1 | \tau_2 \rangle \tag{36}$$

For the implementation we chose to avoid the computation of $\sigma[\tau]$ and $\tau[\sigma]$. This can be done because both bases are equivalent, as we will show it in the next section. We introduce an alternative inner product that applies to a pair of the two equivalent sources (σ, τ) that we note $\sigma\tau$:

$$\langle \sigma\tau_1 | \sigma\tau_2 \rangle = \frac{\alpha}{2} \int_{M \in S} \left(\sigma_1(M) \tau_2(M) + \sigma_2(M) \tau_1(M) \right) \, \mathrm{d}S \tag{37}$$

$$= \langle \sigma_1 | \sigma_2 \rangle = \langle \tau_1 | \tau_2 \rangle \tag{38}$$

Let us notice that this alternative inner product naturally ensures the numerical symmetry of the inner-product.

4.5 Effect of initial basis orthonormalization

4.5.1 Equivalence of the two orthonormalized bases

The choice of the initial bases implies that the vectors σ^0_{km} and τ^0_{km} produce the same field. By using induction, we will now show that the Gram-Schmidt orthonormalization process with respect with inner products (34) and (35) also preserves this property for σ_{km} and τ_{km}.

The basis of the induction is a direct translation of the choice of initial bases (11), (12), (18) and (19). For the simplicity of the demonstration, we temporarily switch the two indices k and m for a single index, which represent the order in which the vectors are orthonormalized. This order is chosen in order to respect (26), i.e. the vectors are orthonormalized in the order of the harmonic order (starting with the three dipolar vectors, then the five quadrupolar ones, etc.). Let's now consider the q^{th} iteration of the Gram-Schmidt orthogonalization:

$$\sigma'_q = \sigma^0_q - \sum_{i=1}^{q-1} \frac{\langle \sigma^0_q | \sigma'_i \rangle}{\|\sigma'_i\|^2} \sigma'_i \tag{39}$$

$$\tau'_q = \tau^0_q - \sum_{i=1}^{q-1} \frac{\langle \tau^0_q | \tau'_i \rangle}{\|\tau'_i\|^2} \tau'_i \tag{40}$$

The choice of initial bases implies that σ^0_q and τ^0_q produce the same field. As the previous steps are assumed true, σ'_i and τ'_i produce the same field $\forall\, i < q$. We can also deduce that $\langle \sigma^0_q | \sigma'_i \rangle / \|\sigma'_i\|^2 = \langle \tau^0_q | \tau'_i \rangle / \|\tau'_i\|^2 \quad \forall\, i < q$ by using (36). From the three previous statements we can conclude that σ'_q and τ'_q are the same linear combinations of vectors that produce the same field.

We now retrieve the vectors of the new bases through the normalization step:

$$\sigma_q = \frac{\sigma'_q}{\|\sigma'_q\|} \quad ; \quad \tau_q = \frac{\tau'_q}{\|\tau'_q\|} \tag{41}$$

As we have shown that σ'_q and τ'_q produce the same field , this also implies that $\|\sigma'_q\| = \|\tau'_q\|$. Thus, σ_q and τ_q also produce the same field, so the step of the induction is verified.

As a consequence, for a given source and choice of enclosing surface, there exist equivalent CD σ and NDD τ. For all k and m, as the vectors σ_{km} and τ_{km} produce the same field we can write $\langle \sigma_{km} | \sigma \rangle = \langle \tau_{km} | \tau \rangle$. Thus, the coefficients c_{km} are the same for both bases.

4.5.2 Ensured decreasing law for the field

The bases $\{\sigma^0_{km}\}$ and $\{\tau^0_{km}\}$ are orthonormalised with respect to the inner product (37) to get the bases $\{\sigma_{km}\}$ and $\{\tau_{km}\}$ that naturally respect property (22) because of (26). This property implies that the scalar magnetic potential ϕ_{km} produced by the new vectors σ_{km} or τ_{km} decreases at least as fast as $1/r^{k+1}$. Outside the BS, the first sum of the spherical decomposition of the scalar potential ϕ_{km} starts at order k:

$$\phi_{km}(P) = \frac{1}{4\pi} \sum_{k'=k}^{\infty} \sum_{m'=-k'}^{k'} \frac{Y_{k'}^{m'}(P)}{r_P^{k'+1}} \frac{\langle \sigma\tau_{km} | \sigma\tau^0_{k'm'} \rangle}{\alpha} \tag{42}$$

This property is illustrated in 2D on Figure 3, where the orthonormalization effect is clearly evident by the emergence of the order k spatial periodicity of the 2D circular harmonic field produced by τ_k.

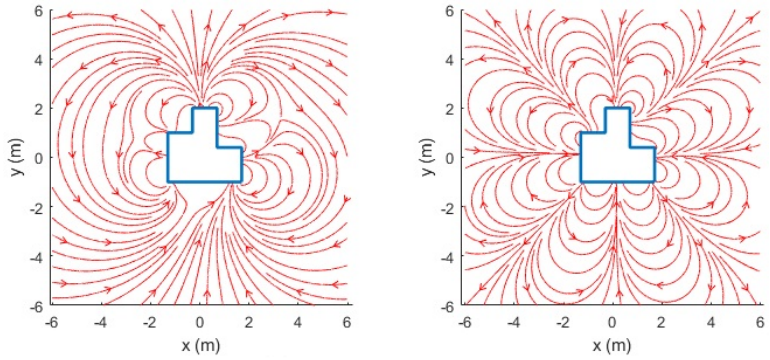

Figure 3: 2D spatial representation of a fourth order source vector ($k = 4$), field lines (red) produced by the NDD on a non-circular surface S (blue), before the orthonormalization (left) and after (right).

Source: Figure created by authors

4.6 Relation between a_{km} and c_{km}

To find the relation between the spherical harmonic coefficients a_{km} for the field and the source harmonic coefficients c_{km} for the equivalent sources, we insert Eqs. (15) and (16) in Eqs. (28) and (29), so that from Eq. (26) we get:

$$a_{k'm'} = \sum_{k=1}^{k'} \sum_{m=-k}^{m'} c_{km} \frac{\langle \sigma\tau^0_{k'm'} | \sigma\tau_{km} \rangle}{\alpha} \tag{43}$$

$$= \sum_{k=1}^{k'} \sum_{m=-k}^{m'} c_{km} \frac{\langle \sigma^0_{k'm'} | \sigma_{km} \rangle}{\alpha} \tag{44}$$

$$= \sum_{k=1}^{k'} \sum_{m=-k}^{m'} c_{km} \frac{\langle \tau^0_{k'm'} | \tau_{km} \rangle}{\alpha} \tag{45}$$

This means that knowing all source harmonic coefficients c_{km} up to an order gives all spherical harmonic coefficients a_{km} up to the same order. This expression is equivalent to a triangular linear system that links all source harmonic coefficients c_{km} up to a certain order K to all the corresponding spherical coefficients a_{km} up to the same order K. As the diagonal of this system has no zeros, it can be inverted to find a similar triangular relation that gives the source harmonic coefficients c_{km} up to a certain order K knowing the spherical harmonic coefficients a_{km} up to the same order K.

4.7 Choice of coefficient α

The coefficient α is chosen in order to have the equality between the spherical harmonic coefficients a_{km} and the source harmonic coefficients c_{km} for the first order ($k = 1$).

Let us call V the volume inside the surface S. Using Green-Ostrogradski theorem we can write (37) for vectors of first order of the initial basis:

$$\left\langle \sigma\tau^0_{1,m} | \sigma\tau^0_{1,m'} \right\rangle = \alpha \int\limits_{M \in V} \boldsymbol{\nabla}\left(rY_1^m\right) \cdot \boldsymbol{\nabla}\left(rY_1^{m'}\right) dV \tag{46}$$

Because of the choice for Y_k^m (see Eq. (3)) we have $\|\boldsymbol{\nabla}(rY_1^m)\| = 1$. Knowing that for $m \neq m'$ $\boldsymbol{\nabla}(rY_1^m)$ and $\boldsymbol{\nabla}(rY_1^{m'})$ are orthogonal, we can write:

$$\left\langle \sigma\tau^0_{1,m} | \sigma\tau^0_{1,m'} \right\rangle = \alpha V \delta_{mm'} \tag{47}$$

with $\delta_{mm'}$ the Kronecker symbol.
As the first three vectors of the initial basis $\{\sigma\tau^0_{km}\}$ ($k = 1$) are already orthogonal, we can write the corresponding vectors of the orthonormalized basis $\{\sigma\tau_{km}\}$:

$$\sigma\tau_{1,m} = \frac{\sigma\tau^0_{1,m}}{\|\sigma\tau^0_{1,m}\|} \tag{48}$$

By replacing in (43) we finally obtain:

$$a_{1,m} = c_{1,m} \frac{\|\sigma\tau^0_{1,m}\|}{\alpha} = c_{1,m} \sqrt{\frac{V}{\alpha}} \tag{49}$$

In order to have $a_{1,m} = c_{1,m}$ for the three coefficients of the first order we thus choose $\alpha = V$.

4.8 Numerical implementation of the bases

The continuous integrals presented in the previous sections are numerically implemented. The surface where the quantities are computed is then discretized through a mesh, and the quantities represented on interpolation functions. The CD are constructed using the same functions that are usually used for the magnetic flux density. We thus use the same shape functions to interpolate those distributions, 0-order shape functions that allows the discontinuities when breaking the surface normal.

The NDD are constructed using the same functions that are usually used for the scalar potential. We thus use the same shape functions to interpolate those distributions, linear nodal shape functions that ensure the continuity of these distributions along the surface.

The values of the initial bases are taken at the centers of the elements for the CD initial basis and at the nodes for the NDD initial basis.

The orthonormalized bases are constructed using modified Gram-Schmidt orthonormalization (Golub and Loan 2013, pp. 254–256). The numerical instability of the orthonormalization process leads to a loss of orthogonality beginning at order 20, for the surface used for validation in Section 5 (see Fig 4a). We reorthonormalize the bases with the same method to improve the orthogonality up to the 29^{th} order (see Fig. 4b), the 30^{th} order still presents a loss of orthogonality.

This loss of orthogonality is critical for the precision of the projection of a source distribution. Without reorthonormalization, the error on the field produced by the projected distribution does not decrease anymore when increasing the truncation order, and the error eventually increases (see Fig. 5). As the loss of orthogonality mainly appears for high orders of truncation, most of the issue will occur when computing the magnetic field in the close proximity of the surface.

Regarding the computation of the field from the obtained single-layer and double layer potentials, let us remember that an analytical expression is available for the single-layer potentials and its derivative when using piece-wise constant interpolation functions (Durand 1964, pp. 243–246) whereas a numerical computation with a 4-point Gauss quadrature is used for the double-layer potentials and its derivative, as well as the computation of the inner product integral. Consequently, for a same accuracy of representation, the field computed for the NDD may be less accurate than the field computed for the CD. In the case of the double-layer potentials and its derivative, the singularity of the integral is solved by shifting the Gauss scheme.

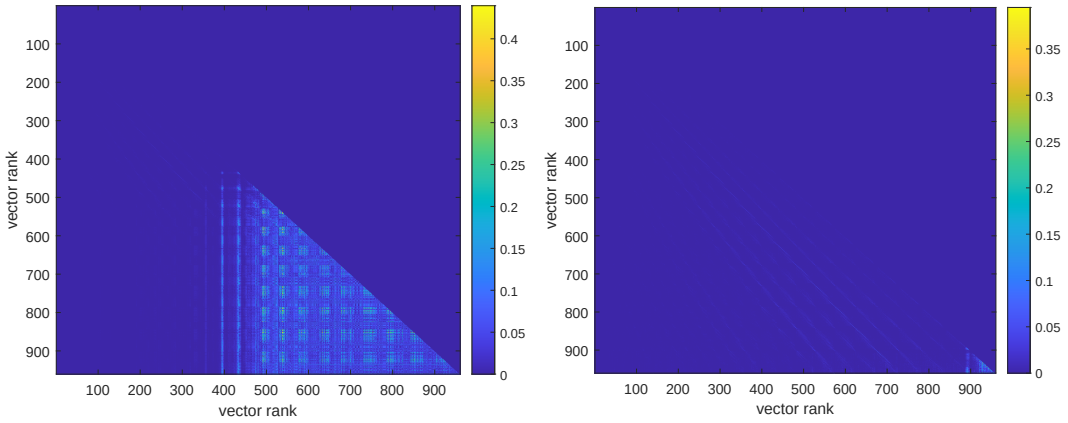

(a) Gram matrix without reorthonormalization (b) Gram matrix with two reorthonormalizations

Figure 4: Gram matrix of the basis $\{\sigma\tau_{km}\}$, constructed using modified Gram-Schmidt orthonormalization, on the surface used for validation in Section 5 .

Source: Figure created by authors

5 Numerical application

5.1 Description of the sources

We consider a source composed of 4 dipoles of intensity 1 Am^2 oriented along the negative z-axis. They are situated at coordinates $-0.5\times0.5\times0.5$ m, $0.5\times0.5\times0.5$ m, $0.5\times-0.5\times0.5$ m and $0.5\times-0.5\times-0.5$ m. Each dipole is equivalent to an off-center multipolar expansion as in (1) and (2) where the only non-zero coefficient is $a_{10} = -1$ Am^2.

From these dipoles we can analytically compute the scalar magnetic potential ϕ and the field $\boldsymbol{H}$ at any point using Eq. (1) and (2). We can also analytically retrieve the global spherical harmonic expansion of these dipoles by translation of the local spherical harmonic expansions (Beatson and GreenGard 1997).

The chosen surface to enclose the source is a polyhedron built from the union of 5 cubes of 1 m side. Four of them are centered on each dipole, the fifth is centered at coordinates $0.5\times0.5\times-0.5$ m (see the green surface on Fig. 6). Its surface is meshed with 5120 quadrangles (5122 nodes).

The magnetic field produced by the different equivalent source distributions is computed and compared to the analytical field on 282 points distributed on 4 planes, each located 50 cm far from one of the interior surfaces of the polyhedron (see the hexahedrons on Fig. 6).

The boundary conditions, i.e. the surface scalar potential ϕ_S and the normal field H_n, associated to the source are analytically computed and displayed on Figures 7a and 7b. The reference distributions, σ_{ref} and τ_{ref}, shown in Figures 7c and 7d, are determined by solving the discretized integrals (9) and (10) on the elements and nodes of the mesh of the surface S. The number of DoF for the normal field and the CD is 5119 to ensure that the magnetic field is divergence free, the number of DoF for the surface scalar potential and the NDD is 5121 as they are defined up to a constant.

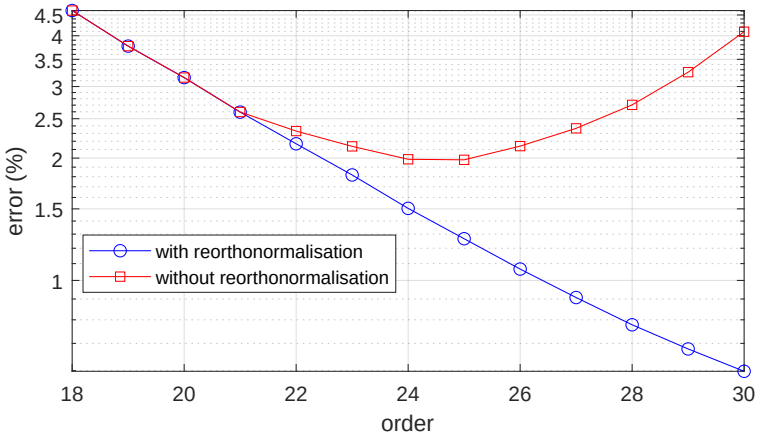

Figure 5: Illustration of the difference of the error of the harmonic NDD basis with and without reorthonormalization. This illustration is taken from the numerical application of the next section, see Fig. 11a for the complete figure with only the reorthonormalized bases.

Source: Figure created by authors

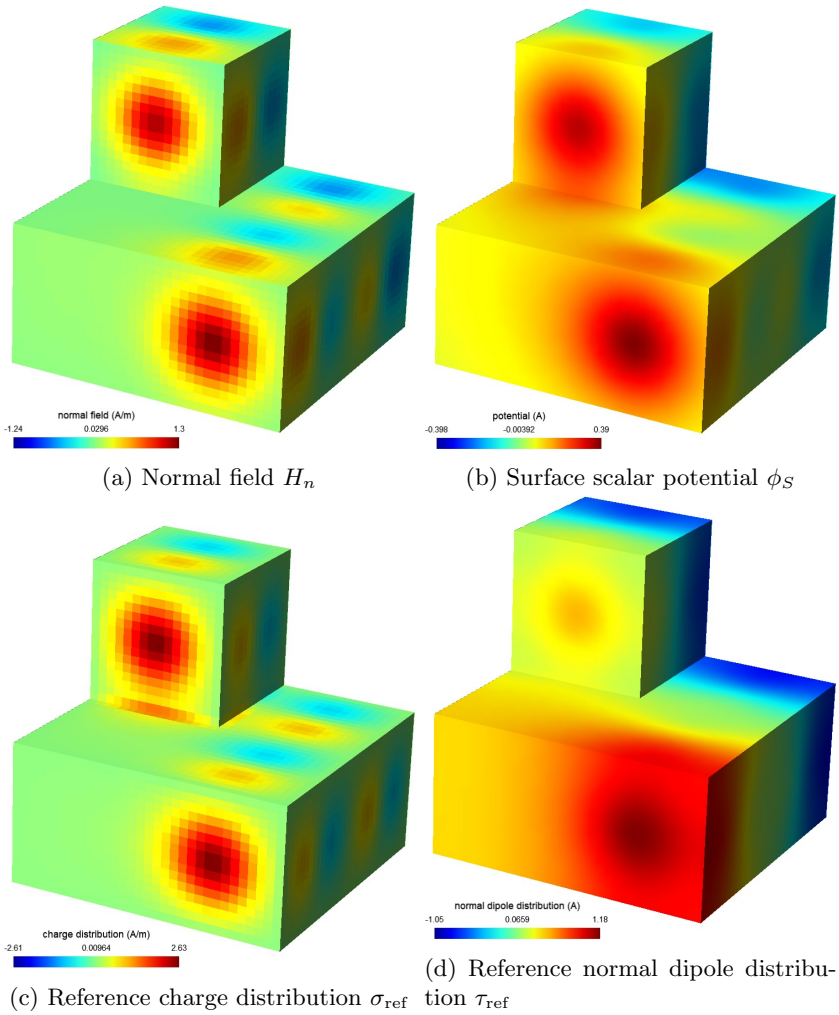

(a) Normal field H_n

(b) Surface scalar potential ϕ_S

(c) Reference charge distribution σ_{ref}

(d) Reference normal dipole distribution τ_{ref}

Figure 7: Boundary conditions (analytical computation) and reference distributions for equivalent sources on the surface (inverse numerical computation).

Source: Figure created by authors

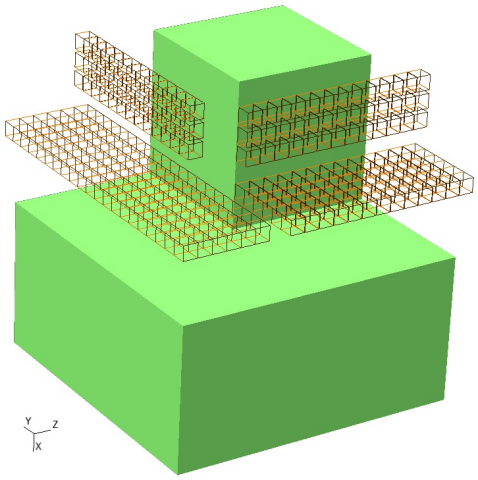

Figure 6: Chosen polyhedron surface and positions of points where the fields produced by the equivalent distributions are compared to the analytical field.

Source: Figure created by authors

As a consequence we do not have analytical expressions for the reference distributions. Let us notice that some sources may provide analytical reference distributions along with analytical field expressions but the simplest physical ones correspond to very low orders (up to 3). For a sake of generality, we preferred to illustrate the performances of our bases on a more multipolar surface source, whose reference distributions are numerically determined, while providing an analytical field (and here also, analytical boundary conditions). When comparing the field produced by our bases in the following, one must distinguish the error of the projection of the reference distribution on the new bases to the one due the reference distribution itself.

5.2 Projection on the orthonormal bases

The reference distributions are projected onto the bases to get the source harmonic coefficients c_{km} (see Fig. 8) using both reference distributions, both orthonormalized bases and the inner product (37). Each order k is described by $2k+1$ coefficients, the total number of DoF is $K(K+2)$ with K the order for the truncation. Here the number of DoF is 960 ($K = 30$) i.e., we obtain a reduction of around one order of magnitude in comparison with the reference equivalent sources unknowns.

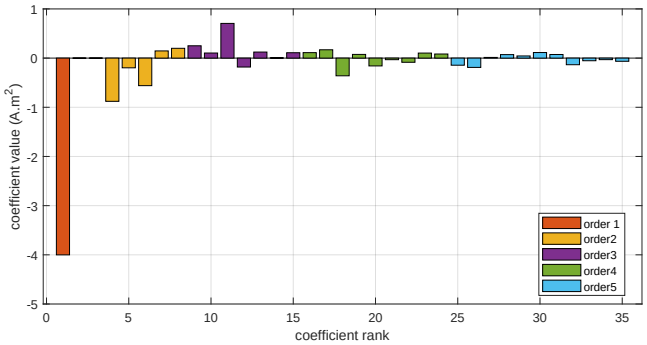

Figure 8: Source harmonic coefficients c_{km} up to order 5.

Source: Figure created by authors

Even if the reference distributions are correctly reconstructed by the bases, the truncation error is particularly visible on the CD (see Fig. 9) as its harmonic representation is smoother than the reference distribution due to the lack of high order information.

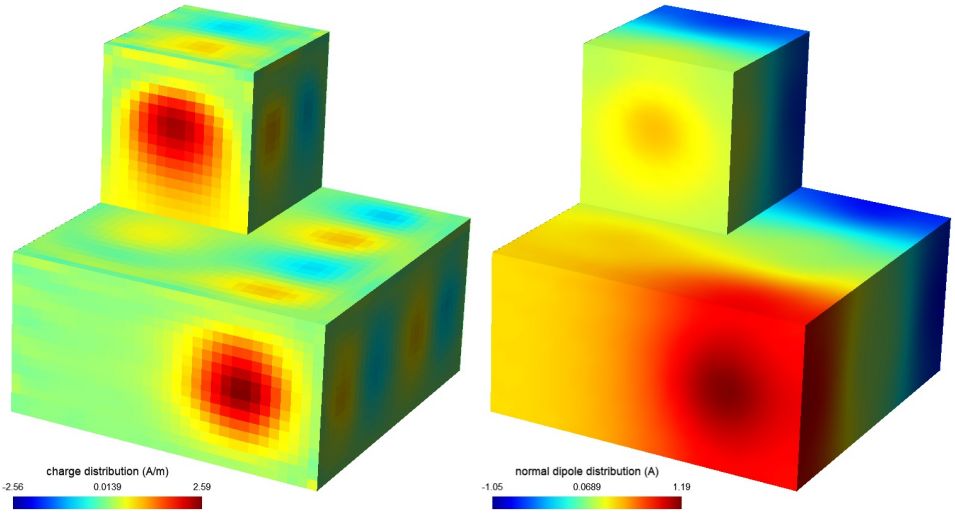

(a) Harmonic charge distribution. (b) Harmonic normal dipole distribution.

Figure 9: Harmonic equivalent sources distributions for a truncation of order 25.

Source: Figure created by authors

5.3 Results outside the Brillouin Sphere

We compute the analytical spherical harmonic coefficients $a_{km}[\text{analytical}]$ with a translation of a multipolar decomposition (Beatson and GreenGard 1997) for each dipole. As we projected the references distribution to the 30^{th} order, we compute the set $a_{km}[\text{analytical}]$ up to the same order. We obtain another set of spherical harmonic coefficients $a_{km}[c_{km}]$ from the source harmonic coefficients c_{km} using Eq. (43).

We normalize the coefficients a_{km} with respect to the radius of the BS ($r_0 = 1.73$ m), we get the normalized coefficients $\overline{a}_{km}$:

$$\overline{a}_{km} = \frac{a_{km}}{r_0^{k-1}} \tag{50}$$

The comparison of those coefficients (see Fig. 10) shows a strong correlation between the two sets of coefficients with less than 0.10 % relative error ε, given by:

$$\varepsilon = \frac{|\overline{a}_{km}[\text{analytical}] - \overline{a}_{km}[c_{km}]|}{\max(|\overline{a}_{km}[\text{analytical}]|)} \tag{51}$$

Thus, this result validates experimentally the good estimation of the c_{km} coefficients by projection of the reference distributions on their associated orthonormalized bases. Moreover, the computation of the field produced by harmonic bases of equivalent sources outside the BS can advantageously be done using the spherical harmonic functions. They are analytically known and less computationally expensive than the computation of the integrals giving the field for a CD or a NDD. As the change of coefficients from source coefficients c_{km} to spherical coefficients a_{km} needs the computation of inner products, the total computational cost is more favorable when computing the field at a high number of points.

5.4 Results inside the Brillouin Sphere

We compute the field $\boldsymbol{H}$ produced by the different representations on the computation planes (see Fig. 6). We will compare the errors ϵ of the different surface representations compared to the analytical field $\boldsymbol{H}_{\text{analytical}}$ (see Fig. 11a) and the errors ϵ' of the harmonic equivalent sources compared to their reference equivalent sources $\boldsymbol{H}_{\text{ref}}$ (see Fig. 11b). This way we separate the errors due to the identification of the reference distributions and of the computation of the field from the error due to the construction of the bases and the projection of the reference distributions.

$$\epsilon = \frac{\|\boldsymbol{H}_{\text{analytical}} - \boldsymbol{H}\|}{\max(\|\boldsymbol{H}_{\text{analytical}}\|)} \tag{52}$$

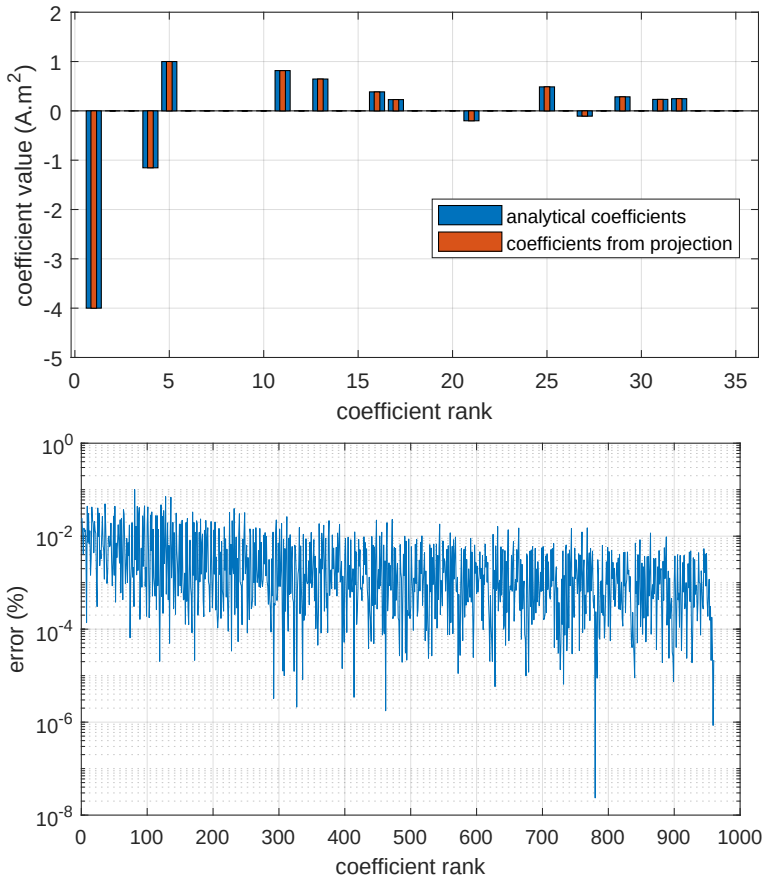

Figure 10: Two sets of normalized spherical harmonic coefficients $\overline{a}_{km}$ for the first five orders (above) and relative difference ε between them (below).

Source: Figure created by authors

$$\epsilon' = \frac{\|\boldsymbol{H}_{\text{ref}} - \boldsymbol{H}\|}{\max(\|\boldsymbol{H}_{\text{ref}}\|)} \tag{53}$$

The maximum error on the four planes for the field computed using the boundary conditions is 0.18%. As those conditions are analytically known, the error is due to the choice of interpolation (0-order shape functions for H_n and linear nodal shape functions for ϕ_S) and the computation of the integrals in (6).

For the reference CD and NDD, the step of identification of those distributions is another source of error. The maximum error of the field is 0.03% for the reference CD and 0.56% for the reference NDD. The fact that the error for the NDD is higher is certainly explained by the difference of integration kernels, the kernels used in the integrals for the identification of the distribution and for the computation of the field are more singular than the ones used for the CD.

When we project the reference distributions onto their bases, we accumulate two more sources of errors that we can not differentiate: a numerical error due to the computation of the inner product and an error due to the truncation of the bases. The error due to the computation of the inner product implies an error on the vector of the bases obtained during the orthonormalization process and an error on the source harmonic coefficients c_{km} obtained by the projection of the reference distributions on the bases.

We have seen Figure 5 that the loss of orthogonality has a negative influence when reaching high orders. Even though we have improved this orthogonality to enhance the quality of the bases, we see on Figure 4b that the orthogonality can still be improved.

Figure 11b shows the evolution of the error due to the truncation. As expected we see a tendency

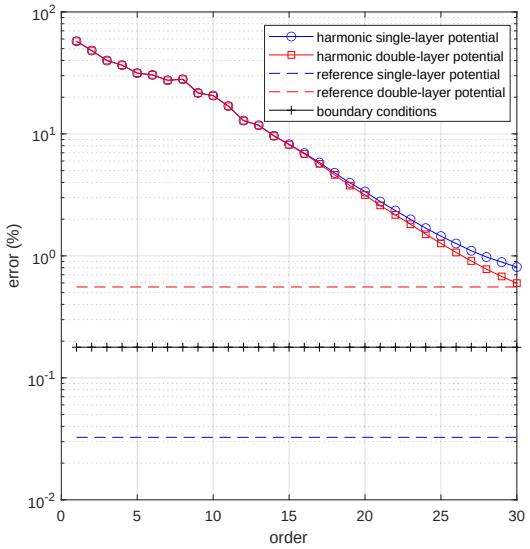

(a) Error ϵ relative to the analytical field.

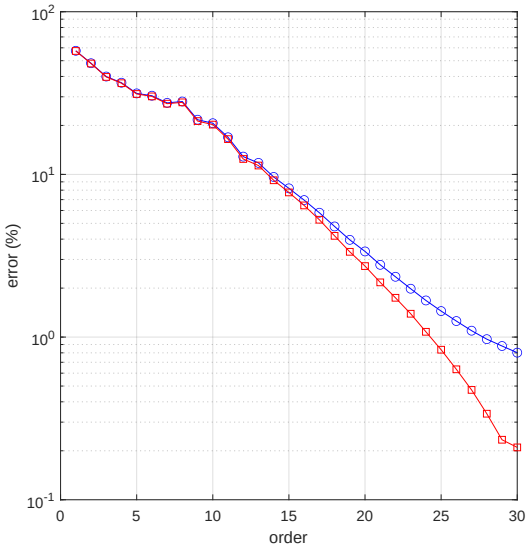

(b) Error ϵ' relative to the field produced by the reference distributions.

Figure 11: Error of the field as a function of the truncation order.

Source: Figure created by authors

to a decrease of the error as the maximum of the error relative to the reference fields decreases down to 0.80% for the CD and 0.21% for the NDD at order 30. Providing that the mesh is dense enough to represent the variation of higher order distributions and that we can orthonormalize the bases with a sufficient precision, we expect this error to continue to decrease when increasing the truncation order. However, the two bases being theoretically equivalent, we expected the two errors to coincide. The fact that the NDD basis shows a better result may be due to the choice of interpolation functions as it is the main difference between the two bases.

On Figure 11a, we see that the behavior of the error of the harmonic source representations relative to the analytical field are similar to the one relative to the reference fields. The error is greater, as it accumulates the error due to the projection and the error due to the choice of representation, and it reaches 0.81% for the CD and 0.60% for the NDD at order 30.

We expect the errors relative to the analytical field ϵ of the harmonic representations to converge to the errors of their respective reference distributions. We can see the beginning of this convergence for the NDD as the error of the harmonic model relative to the reference is low enough so that the error relative to the analytical field is mainly driven by the error induced by the reference distribution. In this case, better accuracy may be achieved by improving the accuracy of the field computation. For the CD representation, the error is mainly driven by the truncation error, the error due to the reference being orders of magnitude lower. In this case, an improvement of the stability of the orthonormalization process is necessary to be able to increase the order of truncation and eventually converge to the same error as the reference.

6 Conclusion

In this paper we have proposed a new harmonic model for field extrapolation which presents the advantage of maintaining the ordered multipolar representation for the equivalent sources and their associated decreasing law outside the BS, and that is valid in all the space around the sources, even inside the BS. We specifically explained the method to construct a multipolar basis for CD, by generalizing the approach introduced by (Legris 1996) for the NDD, and that is now a priori applicable to any other kind of equivalent sources. Moreover, the link between spherical harmonic coefficients that allows an analytical computation of the field outside the BS and the equivalent source harmonic coefficients has been explicitly established. This model has been numerically implemented and validated

by comparison to an analytical example and presents very satisfying performances.

Depending on the proximity of the field evaluation with respect to the source surface, the accuracy of this method at high orders may be dependent on the ability to perform a precise orthonormalization. We have shown that a modified Gram-Schmidt orthornormalisation with reorthonormalization is effective but some numerical instabilities may remain at high orders. A modified Householder orthonormalization (Trefethen 2010) would be more robust but needs an already existing orthonormal reference basis, which is not easy to find (Shao 2023).

Another point of attention concerns the density of the mesh that must be able to catch the spatial variations of the distributions that are directly linked to the truncation order. Let's also note that the performance of the approach is also dependent on the surface regularity, the method leading to some numerical instabilities in the presence of sharp edges.

To conclude, as this model is compact and accurate, it can be used to identify an equivalent source model from very close field measurements, for field extrapolation purpose and also in the context of codes or numerical methods coupling. Further work will deal with the application of this model in an inverse problem approach.

References

Beatson, Rick and Leslie GreenGard (1997). "A short course on fast multipole methods". In: *Wavelets, multilevel methods and elliptic PDEs*. Oxford: Clarendon Press, pp. 1–37.

Bonnet, Marc (1995). *Equations intégrales et éléments de frontière*. CNRS Editions / Eyrolles.

Chavin-Collin, Gireg, Bertrand Bannwarth, Didier Cavallera, Olivier Chadebec, Nicolas Galopin, Gérard Meunier, Olivier Pinaud, and Laure-Line Rouve (Nov. 15, 2021). "A flux-based inverse integral formulation for steel shell magnetization identification". In: *Journal of Magnetism and Magnetic Materials* 538, p. 168275. ISSN: 0304-8853. DOI: 10.1016/j.jmmm.2021.168275.

Cohl, Howard S., A. R. P. Rau, Joel E. Tohline, Dana A. Browne, John E. Cazes, and Eric I. Barnes (Oct. 16, 2001). "Useful alternative to the multipole expansion of 1 / r potentials". In: *Physical Review A* 64.5. ISSN: 1050-2947, 1094-1622. DOI: 10.1103/PhysRevA.64.052509.

Costin, O., R. D. Costin, C. Ogle, and M. Bevis (Jan. 2022). "On the domain of convergence of spherical harmonic expansions". In: *Communications in Mathematical Physics* 389.2, pp. 875–897. ISSN: 0010-3616, 1432-0916. DOI: 10.1007/s00220-021-04262-0.

Durand, Émile (1964). *Electrostatique. Tome I, Les distributions*.

Golub, Gene H. and Charles F. Van Loan (Feb. 15, 2013). *Matrix computations*. JHU Press. 781 pp. ISBN: 978-1-4214-0859-0.

Kybic, J., M. Clerc, T. Abboud, O. Faugeras, R. Keriven, and T. Papadopoulo (Jan. 2005). "A common formalism for the Integral formulations of the forward EEG problem". In: *IEEE Transactions on Medical Imaging* 24.1, pp. 12–28. ISSN: 0278-0062. DOI: 10.1109/TMI.2004.837363.

Legris, Michel (Nov. 22, 1996). "Identification de l'état magnétique d'un système ferromagnétique à partir de mesures du champ proche". PhD thesis. Institut National Polytechnique de Grenoble - INPG.

Shao, Meiyue (2023). "Householder orthogonalization with a non-standard inner product". In: *SIAM Journal on Matrix Analysis and Applications* 44.2, pp. 481–502. DOI: 10.1137/21M1414814.

Stratton, Julius Adams (1941). *Electromagnetic theory*. New York, and London: mcgraw-hill book company Inc.

Tavernier, François, Riccardo Scorretti, Noël Burais, Hubert Razik, and Jean-Yves Gaspard (June 2021). "Real-time numerical dosimetry of low-frequency electromagnetic fields by using multipoles". In: *IEEE Transactions on Magnetics* 57.6, pp. 1–4. ISSN: 1941-0069. DOI: 10.1109/TMAG.2021.3065554.

Trefethen, L. N. (Oct. 1, 2010). "Householder triangularization of a quasimatrix". In: *IMA Journal of Numerical Analysis* 30.4, pp. 887–897. ISSN: 0272-4979, 1464-3642. DOI: 10.1093/imanum/drp018.

Van Hoang, Thi Quynh, Arnaud Breard, and Christian Vollaire (Dec. 2014). "Near magnetic field coupling prediction using equivalent spherical harmonic sources". In: *IEEE Transactions on Electromagnetic Compatibility* 56.6, pp. 1457–1465. ISSN: 0018-9375, 1558-187X. DOI: 10.1109/TEMC.2014.2329601.

Whaler, K. A. and D. Gubbins (June 1, 1981). "Spherical harmonic analysis of the geomagnetic field: an example of a linear inverse problem". In: *Geophysical Journal International* 65.3, pp. 645–693. ISSN: 0956-540X. DOI: 10.1111/j.1365-246X.1981.tb04877.x.